ELSEVIER

Materials Science and Engineering A 465 (2007) 199–210

MATERIALS SCIENCE & ENGINEERING A

www.elsevier.com/locate/msea

Fe_2O_3/aluminum thermite reaction intermediate and final products characterization

Luísa Durães [a,*], Benilde F.O. Costa [b], Regina Santos [c], António Correia [c], José Campos [d], António Portugal [a]

[a] *CEM Group, Department of Chemical Engineering, Faculty of Sciences and Technology, University of Coimbra, Pólo II, Rua Sílvio Lima, 3030-790 Coimbra, Portugal*

[b] *Department of Physics, Faculty of Sciences and Technology, University of Coimbra, Rua Larga, 3004-516 Coimbra, Portugal*

[c] *Centro Tecnológico da Cerâmica e do Vidro, Rua Coronel Veiga Simão, 3020-053 Coimbra, Portugal*

[d] *Thermodynamics Group, Department of Mechanical Engineering, Faculty of Sciences and Technology, University of Coimbra, Pólo II, Rua Luís Reis Santos, 3030-788 Coimbra, Portugal*

Received 24 November 2006; received in revised form 1 February 2007; accepted 19 March 2007

Abstract

Radial combustion experiments on Fe_2O_3/aluminum thermite thin circular samples were conducted. A stoichiometric ($Fe_2O_3 + 2Al$) and four over aluminized mixtures were tested. The combustion products were characterized by X-ray diffraction and Mössbauer spectroscopy and the influence of Fe_2O_3/aluminum ratio on their composition was assessed. The main products were identified as alumina (α-Al_2O_3) and iron (Fe). A significant amount of hercynite ($FeAl_2O_4$) was detected, decreasing with the aluminum excess in the reactants. Close to the sample/confinement interface, where reaction quenching occurs, a non-stoichiometric alumina ($Al_{2.667}O_4$) was observed, being its XRD intensity correlated to the hercynite amount. Fe_3Al intermetallic phase was found in the products of over aluminized mixtures. A reaction mechanism was proposed comprising: (i) Fe_2O_3 reduction to Fe_3O_4 and FeO; (ii) Al oxidation to Al_2O_3; (iii) interaction of the remaining Al with Fe_3O_4 and FeO with formation of iron–aluminates (hercynite) and iron; (iv) for the over aluminized mixtures, incorporation of Al into the iron–aluminates takes place with the formation of iron and alumina and, in parallel, Al reacts with iron to produce intermetallics.

Keywords: Thermite; Iron oxide/aluminum reaction; Products characterization; X-ray diffraction; Mössbauer spectroscopy; Reaction mechanism

1. Introduction

The self-propagating high-temperature thermite reactions are suitable heat sources to several engineering applications and may be applied in advanced materials synthesis. The Fe_2O_3/Al mixture is a classical thermite system which has been used since 1898 on the welding of railway tracks. This reactive system can also be used for cutting and perforation of materials, to produce alumina liners *in situ* for pipes, as a portable heat source, as a high-temperature igniter, as a pyrotechnic heat producer and as an additive to propellants and explosives [1]. More recently, this system is being investigated in environmental protection processes [2], namely for the treatment and recycling of zinc hydrometallurgical wastes [3–5] and for the treatment of by-products of steel industry [6]. Other recent applications of this reactive system are the synthesis of ceramic reinforced metal–matrix composites [7,8], of magnetic granular films [9], of iron aluminides [10–12] and energetic nanocomposites [13–15].

The heat of reaction of the thermite system described by Eq. (1) is sufficient to raise its temperature to very high values (~3000 K), above the melting points or even the boiling points of reactants, intermediate and final products:

$$Fe_2O_3 + 2Al \rightarrow 2Fe + Al_2O_3 + \sim 850\,kJ \quad (1)$$

This kind of combustions has been frequently denominated as "solid flames", "liquid flames" or "gasless combustions" due to the assumption that no gaseous phases evolved from the reaction. However, according to some authors [16], "*The mechanism of the reactions is not simply solid–liquid phase; although only momentarily gaseous, most of the reacting constituents prob-*

* Corresponding author. Tel.: +351 239798737; fax: +351 239798703.
E-mail address: luisa@eq.uc.pt (L. Durães).

0921-5093/$ – see front matter © 2007 Elsevier B.V. All rights reserved.
doi:10.1016/j.msea.2007.03.063

ably pass through the vapor phase, and the particles of the mixture react primarily in that phase, so far as aluminum and oxygen are concerned, only returning to liquid and solid after their combination." The chemical composition and phases of the reaction products are mainly dependent on the reactants composition, reaction extent and cooling conditions. The combustion products of Fe_2O_3/Al thermite comprise, at least, one heavy metallic phase (reduced metallic iron, intermetallics) and a light ceramic phase (Al_2O_3). Since these phases are mutually insoluble and have very different densities, some phase separation occurs during cooling. This step influences the structure of the final products. The high temperature of the combustion front promotes the self-purification of products, releasing: (i) gases adsorbed on reactant particles surface; (ii) low-volatile compounds dissolved/mixed in the reactants during manufacturing; (iii) volatile sub-oxides originated by incomplete thermite reaction [17].

A better knowledge and control of this exothermic reaction is fundamental for the synthesis of tailored materials and/or improvements of its energy applications. Although, the experimental investigation of the reaction mechanism and structures arrangement during cooling is difficult, due to the extreme conditions present, namely, high temperature, high reaction velocity, high heating and cooling rates, and also to the occurrence of interacting physical and chemical phenomena, such as phase changes and diffusion of reactants and products, nucleation and grain growth, solid-phase dissolution, radiative heat transfer and others. This explains why the reaction mechanism of the Fe_2O_3/Al thermite in the self-propagating high-temperature mode (vd. Section 2) is so scarcely studied in the literature.

In this work, the products formed during the Fe_2O_3/Al thermite radial combustion were characterized by X-ray diffraction measurements and Mössbauer spectroscopy. A stoichiometric (vd. Eq. (1)) and four over aluminized mixtures were used, to study the influence of reactants ratio on the reaction mechanism. The combustion experiments were performed on thin circular samples, which were confined in stainless steel circular boxes with upper PMMA lids. To investigate the intermediate products of reaction, the products formed close to the stainless steel confinement surface were analyzed by X-ray diffraction. Due to the high thermal conductivity of stainless steel, the reaction/crystallization in this boundary was partially quenched by the heat losses to the surroundings.

2. Background: Fe_2O_3/Al thermite reaction mechanism and products

Generally, the Fe_2O_3/Al thermite reaction is ignited by an external energy source or induced by mechanical means (ball milling, friction, compression shear). In the first case, the energy source initiates a self-sustained highly exothermic combustion wave which propagates through the sample without any additional energy input. If the energy is abruptly discharged on a confined part of the reactant mixture (heated resistive wire, electric spark, laser beam), the reaction proceeds in the self-propagating high-temperature mode. If it is uniformly applied to all the sample volume (furnace), the thermal explosion mode will occur. In the case of mechanical synthesis, the diffusion of reactants is achieved by their intimate mixing at the atomic level, promoted by the repeated fracture and welding of the components at near room temperature. In this work the reaction proceeds in the self-propagating high-temperature mode. Some works can be found in literature concerning the Fe_2O_3/Al thermite reaction mechanism and products for this mode of propagation.

In 1979, Korchagin and Podergin (vd. [18–20]) used high-temperature diffraction electron microscopy to observe the interaction between hematite particles (α-Fe_2O_3) and an aluminum film. They suggested the following reaction mechanism:

$$3Fe_2O_3 \rightarrow 2Fe_3O_4 + (1/2)O_2 \quad (2)$$

$$Fe_3O_4 + (2/3)Al \rightarrow 3FeO + (1/3)Al_2O_3 \quad (3)$$

$$FeO + Al_2O_3 \rightarrow FeAl_2O_4 \quad (4)$$

They also suggested reactions described by Eqs. (5)–(7), but they discarded their occurrence since no reduced metallic iron was detected in the products:

$$(1/2)Fe_3O_4 + Al \rightarrow Fe + (1/2)FeAl_2O_4 \quad (5)$$

$$2FeO + Al \rightarrow (3/2)Fe + (1/2)FeAl_2O_4 \quad (6)$$

$$(1/2)FeAl_2O_4 + (1/3)Al \rightarrow (1/2)Fe + (2/3)Al_2O_3 \quad (7)$$

In the late 1990s, a research group of Cagliari University published an extensive work on Fe_2O_3/Al thermite reaction mechanism and products [18–23]. They performed the self-propagated reaction with and without the combustion front quenching technique, testing different amounts of alumina and silica as additives (up to 25 wt.%) in air and argon atmospheres. The reactants were mixed in stoichiometric ratio and the samples density was 50–60% of their theoretical maximum density (TMD). They concluded that the environment, in the self-propagating high-temperature mode, did not influence the composition of the reaction products, due to the very fast reaction. They used alumina and silica additives to mitigate the temperature increase. From their results it is clear that the additives play a role in the reaction scheme. When alumina was used, without quenching they detected Al_2O_3, Fe and $FeAl_2O_4$ as products, whereas with quenching they detected additional Fe_2O_3, Al, Fe_3O_4 and FeO. Two different forms of alumina were found: the additive and the one formed during reaction and identified as corundum (α-Al_2O_3). A mechanism of three steps was proposed:

- Step 1: reduction of Fe_2O_3 to iron oxides with lower oxidation states, according to Eq. (2) and

$$Fe_2O_3 \rightarrow 2FeO + (1/2)O_2 \quad (8)$$

- Step 2: interaction of Fe_3O_4 and FeO with Al and Al_2O_3 (additive), originating melted iron–aluminates ($xFeO{\cdot}yAl_2O_3$, including hercynite–$FeO{\cdot}Al_2O_3$) and Fe, according to Eqs. (4)–(6).
- Step 3: crystallization and grain growth of corundum and hercynite from the melt.

Table 1
Summary of literature on the Fe_2O_3/Al thermite reaction products and mechanism, with induction/propagation modes different from the self-propagating high-temperature technique

Author	Experimental conditions	Products found	Proposed mechanism
Mei et al. [25]	$Fe_2O_3 + 2Al$ heated in a furnace to 960 and 1060 °C, at 10 °C/min, in Ar	Fe_3O_4, Al, Al_2O_3 at 960 °C and Fe, Al_2O_3, $FeAl_2O_4$ at 1060 °C	$9Fe_2O_3 + 2Al \rightarrow 6Fe_3O_4 + Al_2O_3$ $Fe_2O_3 \rightarrow 2FeO + (1/2)O_2$ $FeO + Al_2O_3 \rightarrow FeAl_2O_4$ $Fe_2O_3 + 2Al \rightarrow Al_2O_3 + 2Fe$ $3Fe_2O_3 + 2Al \rightarrow 5FeO + FeAl_2O_4$
Cao et al. [19] and Concas et al. [21]	$Fe_2O_3 + 2Al$ reaction, in presence of 25 wt % of alumina, induced by ball milling, in air and Ar, with different energy levels and milling times	Ar: Fe, Al_2O_3 and residual $FeAl_2O_4$, for long times; maximum $FeAl_2O_4$ amount at medium times; Fe–Al alloy appeared with low energy Air: Fe, Al_2O_3, $FeAl_2O_4$ for long times; maximum Fe amount at medium times	Ar: same as for self-propagating high-temperature mode (vd. above in the same work) + Eqs. (3) and (7) Air: environmental O_2 as reactant in the previous reaction scheme (re-oxidation of Fe; more $FeAl_2O_4$)
Matteazzi and Le Caër [26][a]	$Fe_2O_3 + 2Al$ reaction induced by ball milling in Ar and N_2	α-Al_2O_3, α-Fe, Fe–Al solid solution, $FeAl_2O_4$, Fe–Al_2O_3 solid solution, $Fe_{3-x}Al_xO_4$	$FeAl_2O_4$ is an intermediate product of reaction
Matteazzi and Alcalà [27][a]	$Fe_2O_3 + 2Al + 0.7Al_2O_3$ reaction induced by ball milling in Ar for several milling times	0.33 h: α-Al_2O_3, α-Fe, $FeAl_2O_4$, Fe–Al_2O_3 solid solution, Fe_3O_4, Fe_2O_3, Al 2.5 h: α-Al_2O_3, α-Fe, $FeAl_2O_4$, Fe–Al_2O_3 solid solution 8 h: same as before and weak alloying of Fe with Al	Transient formation of $FeAl_2O_4$ due to Fe^{2+} (from Fe and Fe_2O_3) reacting with Al_2O_3; decrease in $FeAl_2O_4$ for higher milling times due to Eq. (7); Fe dissolves in Al_2O_3, forming Fe–Al_2O_3 solid solution
Basset et al. [28][a]	$Fe_2O_3 + 2Al$ reaction induced by ball milling, during 2 and 6 h, in N_2 and air	N_2—2h: α-Fe, χ-Al_2O_3, k′-Al_2O_3, α-Al_2O_3, $FeAl_2O_4$, $Fe_{100-x}Al_x$, Fe clusters in Al_2O_3; Air—2 h: α-Fe, α-Al_2O_3, Fe_2O_3, Fe_3O_4, $FeAl_2O_4$, $Fe_{100-x}Al_x$ ($x = 2.6$), Fe clusters in Al_2O_3 N_2 or air—6 h: α-Fe, α-Al_2O_3, $FeAl_2O_4$, Fe clusters in Al_2O_3	Reaction proceeds faster in N_2 than in air; the decomposition of $FeAl_2O_4$ goes beyond the disappearance of Fe_2O_3; intermediate forms: Fe_3O_4, χ-Al_2O_3, k′-Al_2O_3 and $FeAl_2O_4$
Cuadrado-Laborde et al. [29,30][a]	Fe_2O_3/Al reaction, with 10% excess of Al, induced by ball milling in Ar, with different milling times	α-Fe, α-Al_2O_3, Fe–Al solid solution, $FeAl_2O_4$ for long times	A simple role exchange between Fe and Al occurs, originating the Fe/alumina dispersion
Goya and Rechenberg [31]	Fe_2O_3 + Al reaction induced by ball milling in Ar; milling time = 365 h	$Fe_{0.67}Al_{0.33}$	$Al + Fe_2O_3 \rightarrow 3Fe_{0.67}Al_{0.33} + (3/2)O_2\uparrow$
Shabashov et al. [32]	60 wt.% Al + 40 wt.% Fe_2O_3 reaction induced by: (i) compression shear (6 GPa) + (ii) post-deformation annealing in vacuum (690 K, 30 min)	(i) Fe–Al and Fe–Al–O solid solutions, and α-, γ-Fe_2O_3 (ii) Fe–Al and Fe–Al–O solid solutions, α-Fe_2O_3, Fe_3O_4, α-Fe and Al_3Fe (Only iron compounds were analyzed.)	Qualitatively: (i) Al + α-$Fe_2O_3 \rightarrow Fe_{3-y}O_4$ + $Fe_{1-x}O$ + Fe–O + Al–Fe + Al–Fe–O + α-Fe–Me (ii) previous transformation + $Fe_2O_3 + 2Al \rightarrow Al_2O_3 + 2Fe$

[a] Reaction mechanism was not the aim of this work.

Apart from the observation that product crystals and pores were smaller for samples with lower alumina content (higher combustion temperature), no other variations were observed in the products microstructure.

Kallio et al. [6] treated steel industry by-products, mainly iron oxides mixtures (Fe_2O_3, Fe_3O_4, FeO), by adding aluminum in a stoichiometric amount to promote the thermite reaction. They identified the following products: Al_2O_3, $FeAl_2O_4$, Fe, Fe_3O_4 and FeC. Fe_3O_4 was presumed a remaining reactant and the formation of the carbide was justified by the presence of oil in the reacting mixtures. Independently of the iron oxides ratio in the initial mixture, the same phases were formed. This fact may indicate that Fe_3O_4 and FeO are indeed intermediate products in the Fe_2O_3/Al thermite reaction. In addition, it is possible that the carbide formation can also be due to the contamination by the graphite holder used by these authors. However, the authors should have questioned the presence of an iron carbide with such high amount of carbon, which is very unlikely to occur [24].

Yang et al. [10] prepared Fe_3Al–$Fe_3AlC_{0.5}$ composites in Ar at 5 MPa, according to

$$3Fe_2O_3 + 8Al \rightarrow 2Fe_3Al + 3Al_2O_3 \quad (9)$$

Previously, they added the necessary amount of active carbon powder to obtain 40, 60 or 80 wt.% of $Fe_3AlC_{0.5}$ in the intermetallic phase. The obtained products were the expected composites, with no contamination phases, and α-Al_2O_3 segregated from the intermetallic phase. Dong et al. [8] and Deevi et al. [11] produced composite coatings based on Fe_2O_3/Al self-propagated reaction. Dong et al. [8] ignited a stoichiometric thermite mixture (Eq. (1)) by a plasma spraying flame to form the coating. It consisted primarily of Al_2O_3 and $FeAl_2O_4$, with Fe, FeAl and Fe_3Al as secondary phases. The mechanism suggested for the $FeAl_2O_4$ formation was according to Eq. (4). It was postulated that this compound was formed in sample regions where Fe_2O_3 was in excess. The presence of intermetallics was justified by the contact of Fe and Al melt in sample regions with Al excess. Deevi et al. [11] produced the coatings by reactive plasma spraying of aluminum on carbon steel substrates with a layer of iron oxide on the surface. The iron formed in the thermite reacts with the melted aluminum, originating FeAl or other iron aluminides (characteristic of systems with aluminum excess). Identified products depend on the pre-heat temperature of the substrate and on the number of passes of plasma spraying of aluminum. $FeAl_2O_4$, Al_2O_3, Fe, Fe–Al intermetallics (FeAl, Al_5Fe_2, Fe_3Al, etc.), FeO, Fe_3O_4 and unreacted Al were found in the products.

Since it is not demonstrated that the reaction mechanism depends on the mode of promoting the reaction, some attention was also given to other works investigating the Fe_2O_3/Al reaction products, in which the self-propagating high-temperature mode was not used. They are summarized in Table 1.

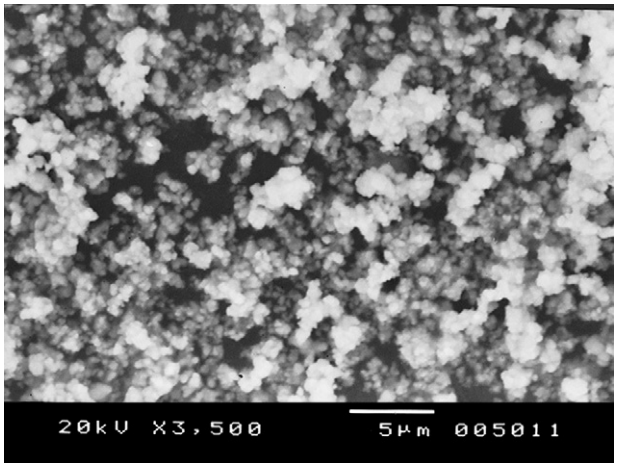

Fig. 1. Scanning electron micrograph of the "Fe_2O_3 Bayferrox 180" reactant powder.

3. Materials and methods

Industrial iron oxide (Bayer) and aluminum (Carob) powders were used to compound the thermite mixtures. The physical properties of these reactants are presented in Table 2. The particle sizes, densities and surface areas were obtained by laser scattering spectrometry (Coulter LS 130), helium pycnometry (Mycromeritics Accupyc 1330) and nitrogen gas adsorption (Mycromeritics ASAP 2000), respectively. Purity data was provided by the manufacturers. Iron oxide and aluminum particles were observed by scanning electron microscopy (JEOL JMS-5310), after coating with a Cu film for improved conductivity. Representative images are shown in Figs. 1 and 2. Iron oxide particles are fine, with regular shape, and easily aggregate in clusters. Aluminum presents mixed coarse and fine particles, with rugged surface, and particles display an irregular flake like shape. Aluminum particles presented a dark grey color and were coated for protection during storage. Mössbauer spectrum and X-ray diffractograms (vd. equipment conditions below) obtained for the reactants are presented in Figs. 3–5. Mössbauer parameters obtained from the fitting to the spectrum are $H = 51.7$ T, IS = 0.341 mm/s and QS = −0.210 mm/s. These parameters are characteristic of hematite (α-Fe_2O_3) [33,34]. The X-ray diffraction patterns can be assigned to hematite (α-Fe_2O_3) and aluminum, for Fe_2O_3 Bayferrox 180 and Al Black 000 India, respectively [35].

Reactants were fed in a rotary mixer and mixed for 24 h. The mixtures were further processed in an industrial mixer

Table 2
Reactants properties[a]

Reactants	Particle size, d_{50} and d_{90}–d_{10} (μm)	Density, ρ (kg m^{-3})	BET surface area, A_s (m^2 kg^{-1})	Purity (wt.%)
Fe_2O_3 Bayferrox 180	1.72 ± 0.16, 3.13 ± 0.05 to 0.75 ± 0.08	5062 ± 11	3150 ± 39	96
Al Black 000 India	11.8 ± 0.3, 47.7 ± 1.6 to 1.59 ± 0.10	2700 ± 7	4475 ± 30	89.3

[a] The uncertainties were calculated for a 95% confidence level, except for Brunauer–Emmett–Teller (BET) surface areas in which they were defined by the S.D.

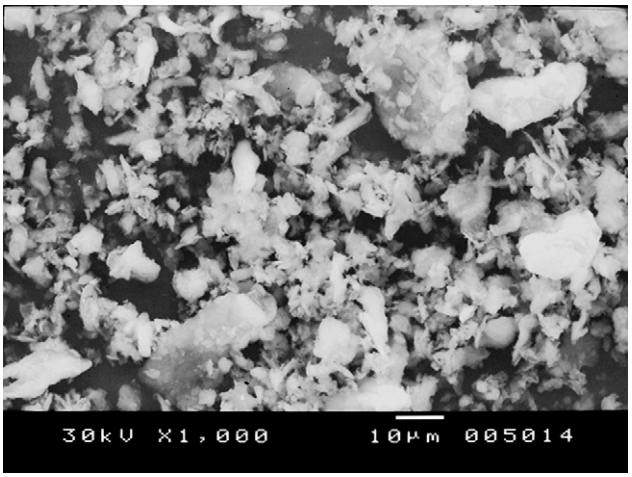

Fig. 2. Scanning electron micrograph of the "Al Black 000 India" reactant powder.

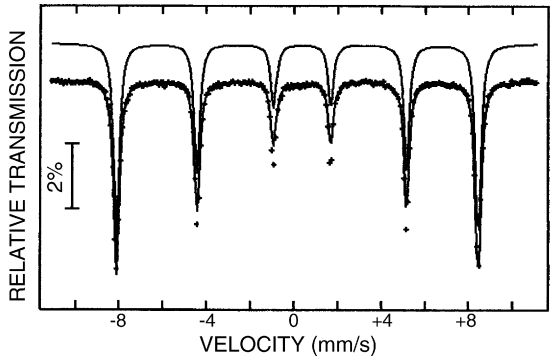

Fig. 3. Mössbauer spectrum, taken at room temperature, of the "Fe_2O_3 Bayferrox 180" reactant. The solid line is the fit to the spectrum and corresponds to hematite (α-Fe_2O_3).

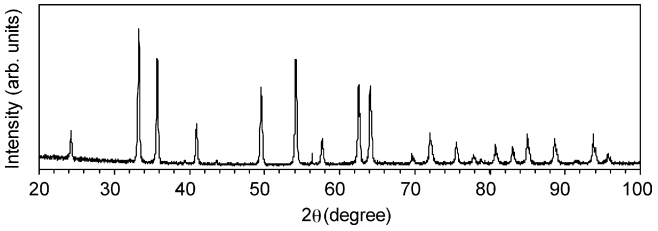

Fig. 4. X-ray diffractogram of the "Fe_2O_3 Bayferrox 180" reactant. Observed peaks fit to the hematite (α-Fe_2O_3, 33-0664) ICDD database pattern [35].

during 30 min, to scrap caked parts. The good distribution of aluminum particles in the iron oxide matrix was confirmed by optical microscopy (microscope Nikon Optiphot HFX-II), as shown in Fig. 6(a). White points, enhanced in Fig. 6(b) by image

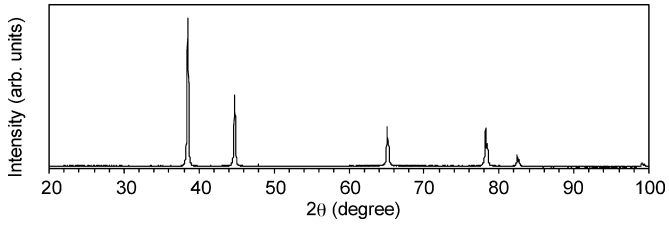

Fig. 5. X-ray diffractogram of the "Al Black 000 India" reactant. Observed peaks fit to the aluminum ICDD database pattern (Al, 04-0787) [35].

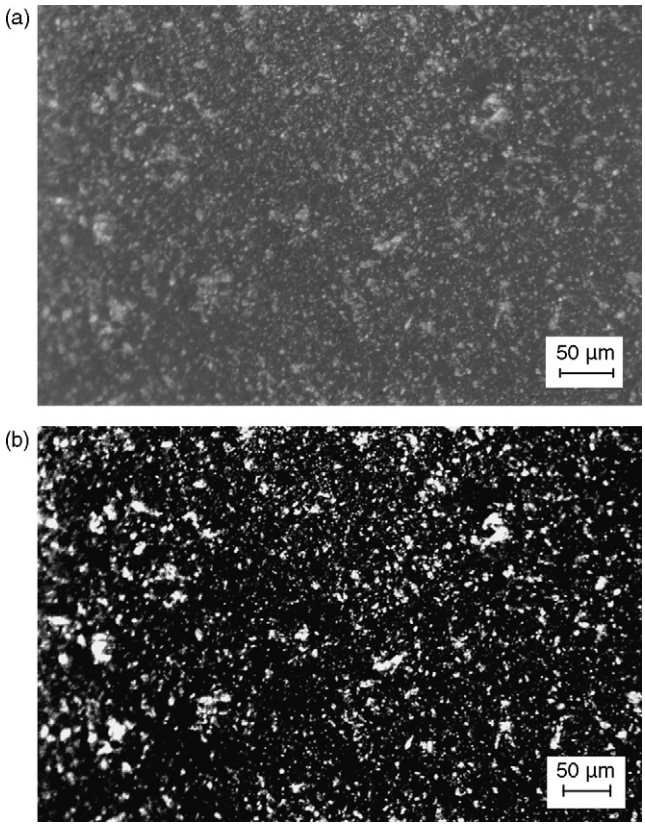

Fig. 6. Typical optical microscopy image obtained in the reactant mixtures observation: (a) as taken and (b) with image treatment to enhance aluminum particles position.

treatment, correspond to the brightness of some aluminum particles. Table 3 presents the mass and molar compositions of the prepared mixtures. The mixtures are identified by the corresponding molar equivalence ratios (ER). T100 corresponds to the stoichiometric ratio.

Combustion experimental set-up and procedure were described elsewhere [36] and is summarized as follows: (i) the thermite mixtures were pressed, in a stainless steel circular box with an inner PMMA lid (vd. Fig. 7), and samples with 1–2 mm thickness and 50–70% TMD density were obtained; (ii) the combustion reactions were initiated at the samples center, by contact with a nichrome wire instantaneously heated via a capacitor discharge; (iii) the radial combustion propagation was monitored by digital video-crono-photography and the combustion temperatures were obtained using tungsten/rhenium thermocouples. Five combustion experiments for each mixture were performed, maintaining the same experimental conditions. Results of the radial combustion propagation profiles and rates and combustion

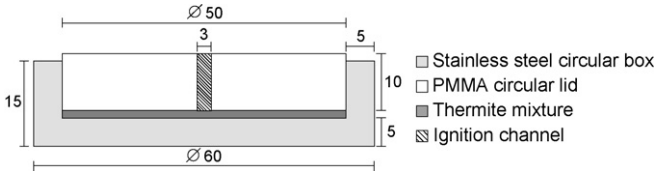

Fig. 7. Experimental sample set-up (front view cut). All dimensions in mm.

Table 3
Thermite mixtures compositions (without impurities)

Mixtures	Fe_2O_3/Al composition (wt.%)	Fe_2O_3:Al composition (mol)	Molar ER[a]	TMD (kg m^{-3})
T100	74.74/25.26	1:2	1.00	4105
T112	72.50/27.50	1:2.24	1.12	4039
T127	70.00/30.00	1:2.54	1.27	3967
T142	67.50/32.50	1:2.85	1.42	3899
T159	65.00/35.00	1:3.19	1.59	3833

[a] (Oxygen necessary for the oxidation of the existing Al to Al_2O_3)/(oxygen actually present in the Fe_2O_3 of the mixture) molar ratio.

temperatures are discussed in Ref. [36]. The chosen radial geometry allows the easy detection of propagation heterogeneities, caused by deficient reactant mixing and/or different levels of compaction, and the testing of self-propagation in conditions of large energy losses to the surroundings, what is ensured by a very low sample thickness. Furthermore, with this geometry, no critical thickness extinction problems arise.

During thermite combustion, the majority of the melted products coalesced and crystallized at preferential points, forming islands glued to the stainless steel surface—slag phase. Same phase separation occurred and part of the melted reduced metallic iron crystallized in droplets. These products were collected in each experiment. To study the intermediate products of the reaction, the plates of the slag phase, were glued to a plasticine base on a metallic support, with the flat surface up—surface in contact with the stainless steel at the end of experiments, filling an X-ray diffraction analysis area. The droplets of reduced metallic iron were also added. These samples, one for each experiment, were analyzed in a Phillips PW 1710 X-ray diffractometer, at 40 kV and 30 mA, from 10 to 100° (2θ) at 1.2°(2θ)/min, using a Cu Kα radiation source (C-Tech Long Fine Focus Cu PW 2773) with λ = 0.154 nm. The representative products for each mixture were obtained by adding all the products collected in combustion experiments of that mixture, including the plates and droplets used in the analysis described above, and crushing them, in an agate mortar grinder, during 2–3 min–bulk products. The five powdered samples obtained were analyzed by X-ray diffraction, on an amorphous support and using the equipment parameters above mentioned. To characterize the chemical states of iron, they were also analyzed by ^{57}Fe Mössbauer spectroscopy, using a standard constant acceleration spectrometer, in transmission geometry, with a 35 mCi Co/Rh source. The analyses were conducted at room temperature. The fitting of the spectra was carried out in two different ways. For T100, T112 and T127 combustion products spectra, a set of Lorentzian lines, determined by least-squares, was used. For T142 and T159 combustion products spectra, a distribution in the hyperfine field and isomer shift was considered for the magnetic part, while for the paramagnetic subspectrum a Lorentzian was considered. The isomer shifts are referred to α-Fe.

4. Results and discussion

X-ray diffractograms in Fig. 8 show the changes in the bulk products formed in the thermite mixtures combustion. A logarithmic intensity scale was used to enhance minor phases and allow its observation. For simplicity, the diffractograms of T112 and T142 products were omitted. The X-ray diffractograms revealed the presence of α-Al_2O_3 and Fe as main phases. The intensity of Fe phase slightly reduces from T100 to T159. $FeAl_2O_4$ and Fe_3Al are also significant phases. Hercynite was widely recognized as an intermediate product of the thermite reaction in the literature (vd. Section 2). In the bulk products, it was detected with higher intensity in the products of mixtures with lower ER, decreasing with the increase in ER and becoming almost absent for ER = 1.59 (T159). Fe_3Al intermetallic phase had an opposite behavior, being detected with higher intensity in the products of samples with higher aluminum content.

Due to the similarity in Fe_3Al (45-1203), FeAl (33-0020) and $Fe_{0.6}Al_{0.4}$ (45-0982) ICDD database patterns [35], the assignment of the Fe_3Al phase was in doubt. However, Mössbauer results presented below indicated the presence of the Fe_3Al phase. Fe–Al intermetallic phases occur when Fe is in contact with melted aluminum [8,10,11], condition met in this thermite process, especially in the case of thermite samples with aluminum in excess.

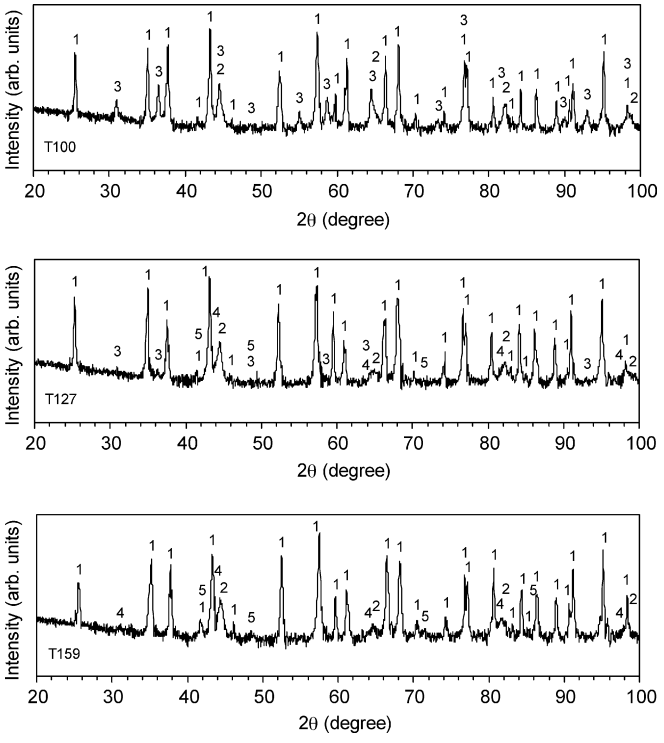

Fig. 8. X-ray diffractograms of bulk products obtained in the combustions of T100, T127 and T159 thermite mixtures: (1) α-Al_2O_3 (10-0173); (2) Fe (06-0696); (3) $FeAl_2O_4$ (34-0192); (4) Fe_3Al (45-1203); (5) Fe_3AlC_x [35].

The iron-rich Fe–Al intermetallic phase, Fe_3Al, is likely to occur in the thermite products since, with the Fe_2O_3:Al equivalence ratios used, the iron produced in thermite reaction is in a much higher amount than the exceeding aluminum. It is known from the literature that the Fe–Al system around the Fe_3Al stoichiometry presents order–disorder phase transformations, which lead to a lack of knowledge of the exact position of aluminum atoms in the iron lattice [37–39]. These transformations are hard to follow by X-ray diffraction and require a high resolution in 2θ axis (high time of analysis). The main differences between the X-ray diffraction patterns for ordered and partially disordered phases are the broadening and decreasing intensity of the peaks in the later case [37,38]. This changes end up by the disappearance of peaks in more disordered states. As the major peaks of the Fe_3Al ordered phase (near 44°, 64° and 81° (2θ)) are very close to the major peaks of iron and, in the obtained diffractograms, the metallic phases have shown low crystallinity, the observation of the Fe_3Al phase major peaks was very difficult. This phase was noticed by the raise of the base line at the angles of the Fe_3Al (45-1203) major peaks and enlargement of the right side of iron major peaks. The appearance of very small broad peaks near 27°, 31° and 98° (2θ) in the samples with a higher amount of this phase confirmed its presence. These signals are better distinguished in Fig. 9 (T159) discussed ahead than in Fig. 8 (T159). So, based on X-ray diffraction results no definite conclusion can be draw about the order state of the Fe_3Al compound, since the peaks of the ordered phase can be observed but they are low and broad. The ^{57}Fe Mössbauer spectra may help to better describe this phase because this technique is sensitive to the local environments around the Fe atoms.

Some carbon was incorporated in the lattice of part of the Fe_3Al phase, originating the Fe_3AlC_x phase, with a diffraction pattern very close to $Fe_3AlC_{0.5}$ (29-0044) and $Fe_3AlC_{0.69}$ (03-0965) ICDD database patterns [35]. The peaks corresponding to this phase were broad (vd. Fig. 8 (T159)) and slightly displaced to the right, when compared to the $Fe_3AlC_{0.5}$ and $Fe_3AlC_{0.69}$ peaks. That may be an indication of a different x value. As expected, the intensity of this phase is directly related to the intensity of the Fe_3Al phase. The presence of C in the system may be attributed to the decomposition during combustion of: (i) the glue film between samples and confinement [36]; (ii) the PMMA lid surface; (iii) the aluminum coating.

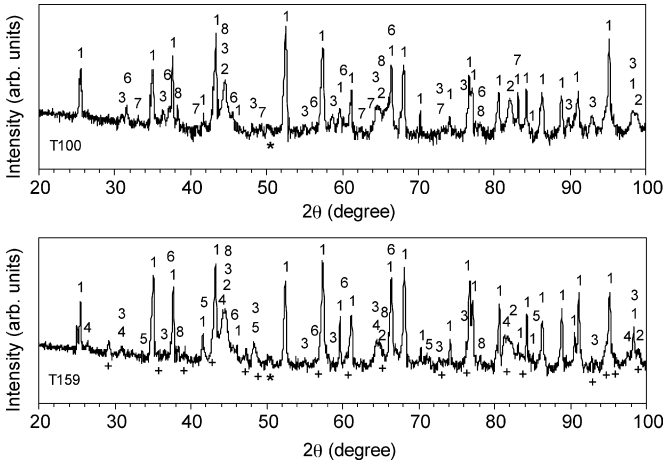

Fig. 9. Typical X-ray diffractograms of products adjacent to the stainless steel confinement surface obtained in the combustions of T100 and T159 thermite mixtures: (1) α-Al_2O_3 (10-0173); (2) Fe (06-0696); (3) $FeAl_2O_4$ (34-0192); (4) Fe_3Al (45-1203); (5) Fe_3AlC_x; (6) $Al_{2.667}O_4$ (80-1385); (7) α-Fe_2O_3 (33-0664); (8) Al (04-0787) [35].

The presence of $FeAl_2O_4$ and Fe_3Al clearly depends on the Fe_2O_3:Al ratio, appearing the first when the oxygen available (i.e. the Fe_2O_3 amount) is above the stoichiometric amount (Eq. (1)) and the second when aluminum is in excess. This confirms what was postulated by Dong et al. [8] (vd. Section 2). The mixtures used in this work were estimated as over-aluminized, with the exception of T100. However, although considering the purity claimed by the manufacturers, the calculated values for ER do not consider some additional oxidation of the aluminum surface during storage and some (low) degree of incompleteness of reaction, common in fast reaction processes. Consequently, experimentally, the stoichiometry was not achieved in T100 composition. In a different paper [36], the combustion rate values obtained for these mixtures were analyzed. It was observed a quasi-linear increase of the combustion rate with the equivalence ratio, in the studied range of equivalence ratios. This was explained by an increase of completeness of thermite reaction. The authors know now that an increase of the thermal conductivity of reactants and products due to the presence of a higher amount of metallic phases in over aluminized samples may also have played a contribution to that increase in the combustion rate [40]. However, as presented in Ref. [36], superimposed to the linear increase of the combustion rate, an enhanced increase of this variable was observed in the range ER = [1.12, 1.27]. It was concluded that the experimental stoichiometric point was placed in this interval and the enhanced increase in the combustion rate was caused by the additional heat of reaction released in an intermetallic formation, according to

$$3Fe + Al \rightarrow Fe_3Al + \sim 67\,kJ \quad (10)$$

This range may also be applied to the present results, although hercynite remains detectable in T142 combustion products. Furthermore, this explains why in the T159 combustion products, the exceeding aluminum is not sufficient to consume all the amount of the produced iron in the thermite reaction, notwithstanding this thermite sample had a Fe_2O_3:Al molar ratio of 1:3.19, higher than the predicted by Eq. (9) (1:2.66) for all iron consumption. It also reinforce the assignment of the Fe–Al intermetallic phase with the highest Fe:Al molar ratio as the most probable intermetallic in the obtained diffractograms.

The X-ray diffraction analysis of products crystallized near the stainless steel confinement surface revealed the same main phases of the bulk products—alumina and reduced metallic iron. $FeAl_2O_4$, Fe_3Al and Fe_3AlC_x were also present with significant intensities and with nearly the same behavior as before. However, it was observed that the hercynite intensities decrease with the ER is less steep. A non-stoichiometric alumina phase – $Al_{2.667}O_4$ – appeared in these results with intensities similar to those of hercynite. Fig. 9 shows typical diffractograms obtained for these boundary products. T100 and T159 mixtures were

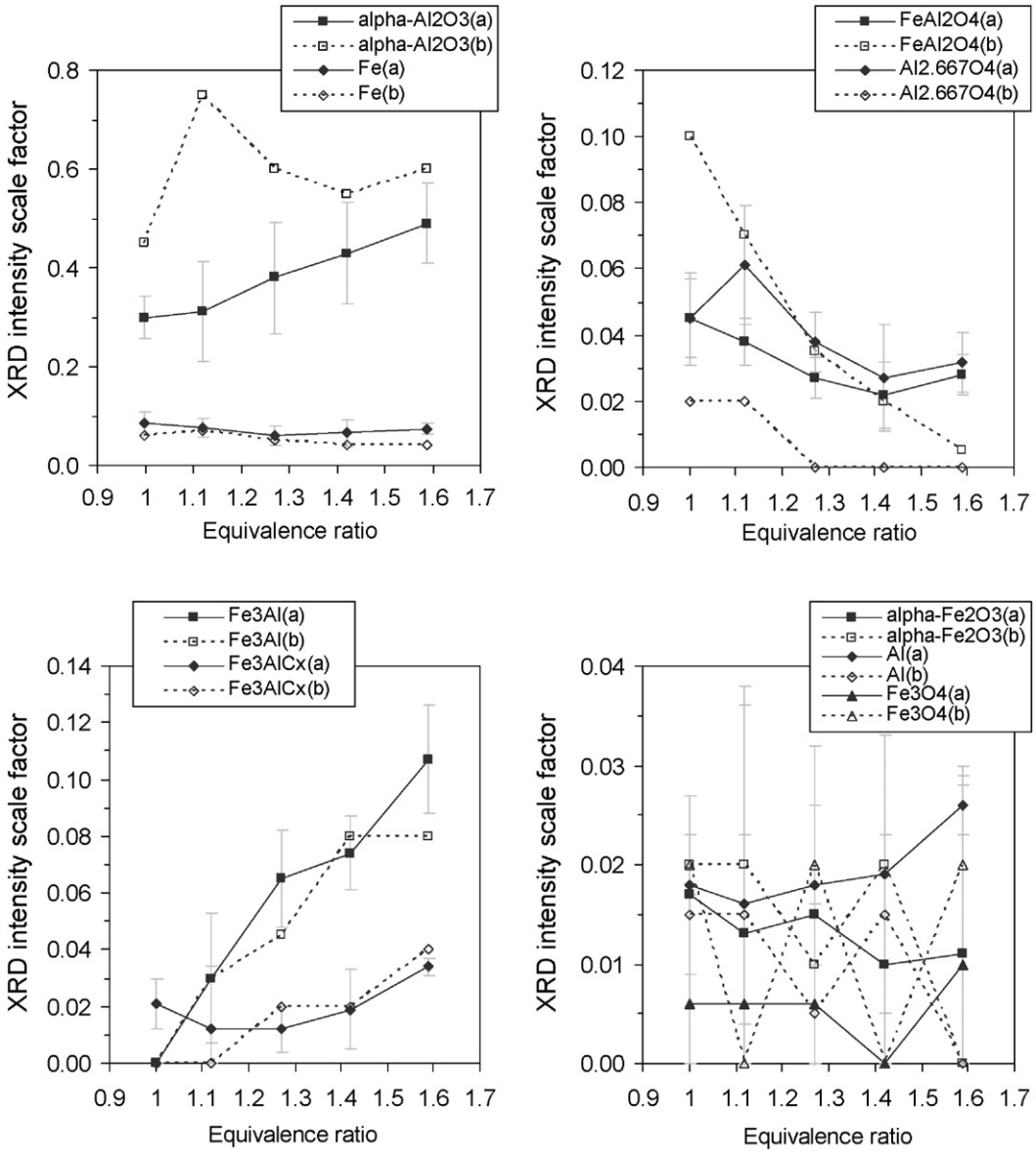

Fig. 10. X-ray diffraction (XRD) intensity scale factors for the phases found in (a) products adjacent to the stainless steel confinement surface and (b) bulk products obtained in the thermite mixtures combustions. The ICDD database pattern of $Fe_3AlC_{0.5}$ was used to find the scale factor for Fe_3AlC_x.

chosen to illustrate the main changes in $FeAl_2O_4$, Fe_3Al, Fe_3AlC_x and $Al_{2.667}O_4$ product phases. The symbol (*) indicates a non-assigned peak. It may be due to some contamination of products by the stainless steel confinement, because $Cr_{0.19}Fe_{0.7}Ni_{0.11}$ (33-0397) and $Ni_{2.9}Cr_{0.7}Fe_{0.36}$ (33-0945) phases [35] show one of their main peaks close to this angle. The symbol (+) (Fig. 9 (T159)) corresponds to the positions of calcite diffraction pattern. This phase appeared in some of the diffractograms collected with a plasticine base to fix the samples. It represents an interference of the plasticine composition.

For each mixture, five combustions were performed, and the corresponding X-ray diffraction analysis of the products crystallized close to the stainless steel confinement surface was done (vd. Section 3). Adjusting, for each phase, the intensities of the major peaks of the ICDD database pattern to the intensities in the diffractogram, an intensity scale factor was found. This scale factor represents the ratio between the intensity of a given phase in the as-measured diffractogram and the intensity of the non-textured ICDD database pattern. Fig. 10 presents these results, with the corresponding 95% confidence level interval. The same adjustment was done in the bulk products diffractograms. As each mixture originated only one analysis (vd. Section 3), no error interval is shown in this case. Since the peak heights depend of the amount and crystallinity of phases, a careful discussion of Fig. 10 should be made, especially in this case where peaks present some broadening and phase overlapping. As stated above, the increase of combustion velocity with ER [36] was associated with an increase in the samples exothermicities, originated by an increase in thermite reaction completeness and superimposing of the intermetallic reaction. Therefore, higher combustion temperatures and more violent propagations are expected in reactive samples with higher amount of aluminum.

The melted products intermixing and spreading were very significant and enhanced in these conditions [36], leading to higher cooling rates and products disintegration that reduced the products crystal growth. Also, the increasing amount of metallic phases with ER increases the thermal conductivity of the samples and favors the cooling process with the same effect on products crystal size. The mentioned products disintegration effect was observed by Dahotre and Nayak [41] and Nayak et al. [42] in the self-propagating combustion of the thermite reaction between Fe_3O_4 and aluminum, which is comparable to the system studied in this work.

Thus, the crystallinity of phases seem to decrease (lower intensity) with higher ER. Any behavior of intensity scale factor increase with ER can be interpreted as an increase in the phase amount. Also, any strong decrease cannot surely be justified only by crystallinity decrease, because the measured combustion properties of mixtures were not very dissimilar. When comparing bulk products with boundary products, it must be considered that the last were exposed to higher cooling rates (quenching) and are expected to have lower crystallinity. For example, α-Al_2O_3 in the boundary products present lower intensity scale factors than the corresponding phase in the bulk products, but could be present in similar amounts. The increase of this phase in the boundary products with ER can be explained by a higher extent of reaction with higher ER. This was not observed in the iron phase because it is formed by the thermite reaction but is partially consumed by the intermetallic reaction. In the bulk products, the increase of α-Al_2O_3 intensity scale factor from ER = 1 to 1.12 is surely related to an higher extent of thermite reaction, that is confirmed by the slight increase also observed on Fe intensity scale factor. The decrease of α-Al_2O_3 intensity scale factor for higher ER > 1.12 does not mean necessarily a decrease in the amount of α-Al_2O_3 since a lowering of crystallinity is known to occur. Therefore, there is an increase in the amount of α-Al_2O_3 in T112–T159 combustion products when compared to T100. For ER > 1.12 the amount α-Al_2O_3 seems to stabilize. This stabilization is not detected for α-Al_2O_3 in the boundary products because, in this case, there is more room for improvement of the reaction extent with the increase in ER. The heat added by the intermetallic reaction improved the thermite reaction. Observed behavior of $FeAl_2O_4$ and Fe_3Al scale factors supports this conclusion. As expected, $FeAl_2O_4$ and $Al_{2.667}O_4$ intensity scale factors did not decrease appreciably with ER in the boundary products. The reaction and/or crystallization were quenched in some degree in this region, leading to higher amounts of intermediate products. $Al_{2.667}O_4$ phase was detected in the boundary products with a significantly higher intensity scale factor than the ones observed for the bulk products. This can be attributed to an incomplete crystallization process of the iron–aluminates and alumina (mechanism proposed in Refs. [18–23]; vd. Section 2, step 3). The ratio 4O/2.667Al ≈ 3O/2Al of aluminas.

Unreacted reactants and Fe_3O_4 were detected with very low intensity scale factors (in the detection limit of the equipment) both in the boundary and bulk products (vd. Fig. 10). Therefore, no consistent comparison of these results is possible. The low intensity observed for Fe_3O_4 was expectable, since this intermediate product is originated in an earlier step of the thermite reaction mechanism (vd. Section 2).

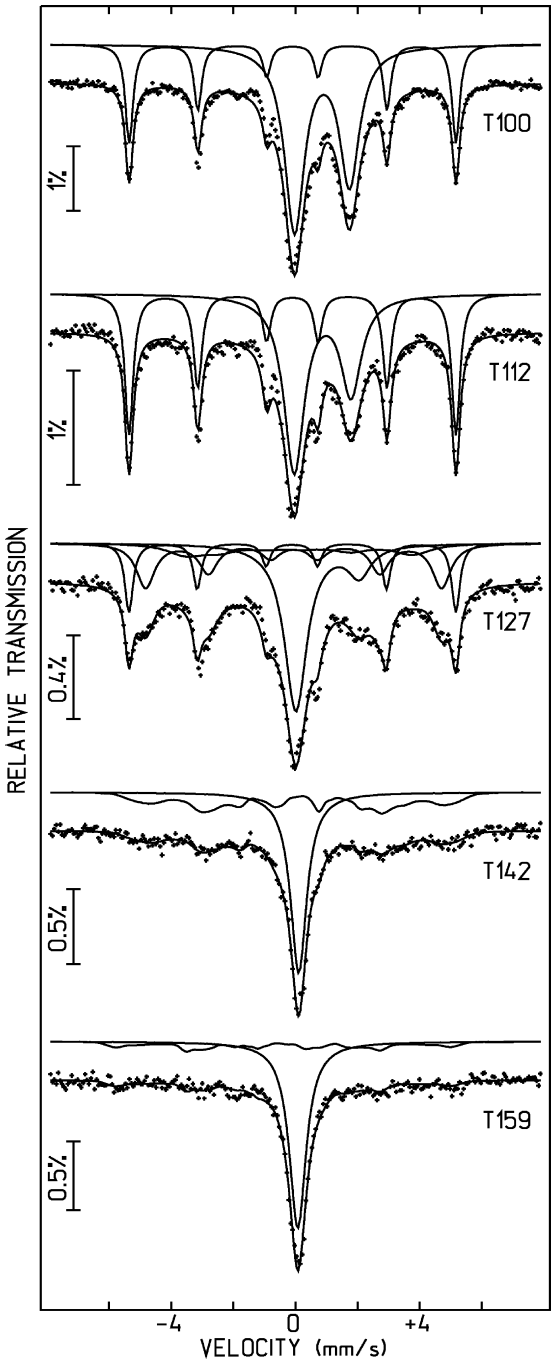

Fig. 11. Mössbauer spectra, taken at room temperature, of bulk products obtained in the combustions of indicated thermite mixtures. Solid lines are the fits to the spectra. Subspectra lines are also included, corresponding to the phases shown in Tables 4 and 5.

Mössbauer spectra of the bulk products at room temperature are presented in Fig. 11 and the fitting parameters are given in Tables 4 and 5. As it is shown, the T100 and T112 combustion products were described by two subspectra, ascribed to α-Fe and $FeAl_2O_4$ phases [19,21,43,44]. The percentage of the later was significant, being 67.7% and 54.5% for each sample, respectively. For the T127 combustion products sample, apart from the

Table 4
Mössbauer parameters fitted to the spectra shown in Fig. 11 and the corresponding S.D.

	Isomer shift, IS (mm/s)	Quadrupole splitting, QS (mm/s)	Magnetic hyperfine field, H (T)	Line width at half maximum, Γ (mm/s)	Relative area, I (%)
T100 combustion products					
α-Fe	0.012 ± 0.002	0.005 ± 0.003	33.0	0.30 ± 0.01	32.3
$FeAl_2O_4$	0.977 ± 0.002	1.797 ± 0.004	–	0.78 ± 0.01	67.7
T112 combustion products					
α-Fe	0.009 ± 0.002	0.005 ± 0.007	33.1 ± 0.1	0.33 ± 0.01	45.5
$FeAl_2O_4$	0.996 ± 0.005	1.858 ± 0.007	–	0.81 ± 0.01	54.5
T127 combustion products					
α-Fe	0.000	0.005 ± 0.002	33.0 ± 0.1	0.32 ± 0.01	19.6
$FeAl_2O_4$	1.09 ± 0.02	1.95 ± 0.03	–	0.85 ± 0.02	38.3
Fe_3Al	0.057 ± 0.002	−0.017 ± 0.010	29.9 ± 0.1	0.72 ± 0.01	28.1
	−0.005 ± 0.001	0.06 ± 0.01	21.6 ± 0.1	1.46 ± 0.02	14.0

The fitting procedure was done by a set of Lorentzians.

two above-mentioned subspectra, there are other two magnetic subspectra ascribed to different sites of Fe in Fe_3Al [33,37–39]. The relative percentage of this compound was 42.1%, which corresponds to a significant part of the sample.

In a perfect ordered Fe_3Al crystalline phase, the component at about 20 T is two times more intense than the component with an H of about 30 T. However, with progressive disordering, the intensity of the 20 T component decreases. When the Fe_3Al phase is disordered, it shows a broad distribution peaked at about 27 T [37,38]. The spectrum obtained in this work for T127 combustion products presents a more intense peak at about 30 T and agrees better with a Fe_3Al disordered phase than with an ordered one. Additionally, the two magnetic sites obtained have a slight electric quadrupole interaction, as observed for disordered Fe_3Al spectra by Lesoille and Gielen [39]. The disordering of the Fe_3Al phase may be associated with composition variations which are not easy to determine.

The asymmetry observed in the quadrupole doublet of hercynite in the three samples above indicates non-stoichiometry of this compound, originated by some substitution of Al with the Fe atoms—$Fe_{1+x}Al_{2-x}O_4$, for x small [19,26]. The percentage decrease of the hercynite intermediate product from T100 to T127 combustion products confirms the results obtained by X-ray diffraction. Simultaneously, the increase of the aluminum content from T100 to T112 mixture, led to an increase of the reduced metallic iron produced. The further increase in aluminum content of the mixtures (T127 mixture) originated an excess of aluminum and the formation of Fe_3Al intermetallic phase. As expected, this led to a decrease of the reduced metallic iron. These observations indicate that T100 did not correspond to experimental stoichiometry, as mentioned above. Furthermore, the range of equivalence ratios given in Ref. [36] for the experimental stoichiometry is validated by the results of this technique.

For T142 and T159 combustion products samples, it was obtained a paramagnetic part and a magnetic background fitted as a distribution of hyperfine field. The paramagnetic part increased from T142 to T159 combustion products, being 43% and 77%, respectively. It can be associated with one or either of the following hypotheses: (i) supermagnetism due to the reduction of the combustion products crystal sizes to nanometric range [28,29] (the higher combustion front velocities observed in these samples, their higher exothermicities and thermal conductivities originated the reducing of the products crystal growth, as explained before); (ii) the dissolution of Fe (and probably the intermetallic as well) in a non-magnetic matrix, like Al_2O_3 [26,28,45] or Al [26,32]. Concerning the hypothesis (ii), nanometric iron particles may be stabilized in the alumina matrix [45] and the coexistence of superparamagnetic and magnetic states of iron is possible in this case, being 10 nm the critical size of iron clusters to exhibit superparamagnetism [9]. The hypothesis above can also be supported by the rather easy way that these two samples were crushed when compared to the others. This is an indication that the crystals of the ductile phases did not grow as much as in the other samples. In X-ray diffraction, a significant broadening of the peaks was not clear due to the superimposing of peaks of different structures. The central paramagnetic peak already appeared in the T127 combustion products spectrum,

Table 5
Mössbauer parameters fitted to the spectra shown in Fig. 11 and the corresponding S.D.

	Mean isomer shift, <IS> (mm/s)	Mean magnetic hyperfine field, <H> (T)	Isomer shift, IS (mm/s)	Line width at half maximum, Γ (mm/s)	Relative area, I (%)
T142 combustion products	0.02 ± 0.02	25.6 ± 0.4	–	–	42.8
	–	–	0.213 ± 0.004	0.64 ± 0.02	57.2
T159 combustion products	−0.037 ± 0.010	26.1 ± 0.5	–	–	23.3
	–	–	0.182 ± 0.005	0.67 ± 0.02	76.7

The fitting procedure was done with a distribution of hyperfine magnetic field and isomer shift for the magnetic part.

but its contribution could not be separated from the hercynite doublet with a variable stoichiometry of this compound. The magnetic part observed in T142 and T159 combustion products samples may be ascribed to Fe_3Al, as the mean hyperfine fields lay in between the values obtained for the two sites of this magnetic compound and mean isomer shifts are also comparable. This magnetic part can also have the contribution of the Fe phase. Iron phases detected with residual intensities by X-ray diffraction, i.e. Fe_3AlC_x, Fe_2O_3 and Fe_3O_4, were not observed in Mössbauer spectra due the limited resolution of Mössbauer spectroscopy.

Considering the discussion above, a qualitative mechanism for the thermite reaction in the self-propagation high-temperature mode is proposed:

(1) With ignition heat (in the ignition period) or heat conducted/radiated from the already reacted layers, Fe_2O_3 is reduced to Fe_3O_4 and FeO, in successive endothermic steps, releasing oxygen at high temperature.
(2) The oxygen formed in step 1 reacts with the melted or vaporized aluminum, forming alumina and releasing high amounts of heat.
(3) Depending on the ratios of Fe_3O_4/Al and FeO/Al (which is determined directly by the reactants ratio and also by the amount of unreacted aluminum and aluminum suboxides lost by vaporization), hercynite is formed by the reactions of Eqs. (4)–(6), where reduced metallic iron is also formed; the products of these reactions are all melted and non-stoichiometric hercynites may appear in this step.
(4) Formed hercynite can crystallize, giving an end-product, or incorporate more aluminum (if it is still available) and forming reduced metallic iron and alumina via Eq. (7); in this last reaction non-stoichiometric aluminas may be formed, depending on the amount of aluminum available.

In this reaction process, if the aluminum is in excess, even if only locally, the iron produced can form intermetallic compounds with the melted aluminum. This reaction may compete in some extent with reaction described by Eq. (7). In this work, the thermite combustion quenching in the samples boundary only affected step 4 of the above mechanism.

5. Conclusions

The products formed in the radial combustion of thin circular Fe_2O_3/Al thermite samples were characterized by X-ray diffraction and Mössbauer spectroscopy. Stoichiometric and over aluminized mixtures were prepared and the influence of the Fe_2O_3/Al ratio on the reaction mechanism was investigated. Alumina (α-Al_2O_3) and reduced metallic iron (Fe) were the main products of reaction, as expected. $FeAl_2O_4$ was found to be an important intermediate product. It was detected in the final products in high amounts due to reaction incompleteness, but its significance decreases with the increase of the aluminum content in the reactant mixtures. A non-stoichiometric alumina phase ($Al_{2.667}O_4$) was present in the samples boundary regions, where heat losses to the surrounding partially quenched the reaction/crystallization. The amounts of these two last phases are correlated and support the hypothesis of a reaction mechanism via iron–aluminates. Fe_3Al intermetallic phase was found in considerable amounts in the combustion products of mixtures with aluminum excess. A reaction mechanism was proposed, considering the different contexts of aluminum availability in the reaction zone.

Acknowledgements

An acknowledgement is due to Margarida Figueiredo for the access to particle size, density and surface area measurement techniques in Labgran and Teresa Vieira and Bruno Trindade for the SEM facility in Led&Mat. The authors also would like to thank to Bruno Trindade and Albano Cavaleiro for the valuable discussions in the revision of this manuscript.

References

[1] S.H. Fisher, M.C. Grubelich, Proceedings of the 24th International Pyrotechnics Seminar, IIT Research Institute Chicago, July 27–31, 1998, pp. 231–286.
[2] G. Cao, R. Orrù, Chem. Eng. J. 87 (2002) 239–249.
[3] R. Orrù, M. Sannia, A. Cincotti, G. Cao, Chem. Eng. Sci. 54 (1999) 3053–3061.
[4] M. Sannia, R. Orrù, A. Concas, G. Cao, Ind. Eng. Chem. Res. 40 (2001) 801–807.
[5] M. Porcu, R. Orrù, G. Cao, Chem. Eng. J. 99 (2004) 247–256.
[6] M. Kallio, P. Ruuskanen, J. Mäki, E. Pöyliö, S. Lähteenmäki, J. Mater. Synth. Process. 8 (2) (2000) 87–92.
[7] N. Travitzky, P. Kumar, K.H. Sandhage, R. Janssen, N. Claussen, Mater. Sci. Eng. A 344 (2003) 245–252.
[8] Y. Dong, D. Yan, J. He, X. Li, W. Feng, H. Liu, Surf. Coat. Technol. 179 (2004) 223–228.
[9] V.G. Miagkov, K.P. Polyakova, G.N. Bondarenko, V.V. Polyakov, J. Magn. Magn. Mater. 258–259 (2003) 358–360.
[10] J. Yang, P. La, W. Liu, Y. Hao, Mater. Sci. Eng. A 382 (2004) 8–14.
[11] S.C. Deevi, V.K. Sikka, C.J. Swindeman, R.D. Seals, J. Mater. Sci. 32 (1997) 3315–3325.
[12] S.P. Chakraborty, I.G. Sharma, A.K. Suri, D.K. Bose, J. Mater. Process. Technol. 115 (2001) 413–422.
[13] A.E. Gash, R.L. Simpson, T.M. Tillotson, J.H. Satcher, L.W. Hrubesh, Proceedings of the 27th International Pyrotechnics Seminar, IIT Research Institute Chicago, July 16–21, 2000, pp. 41–53.
[14] T.M. Tillotson, A.E. Gash, R.L. Simpson, L.W. Hrubesh, J.H. Satcher Jr., J.F. Poco, J. Non-Cryst. Solids 285 (2001) 338–345.
[15] L. Menon, S. Patibandla, K. Bhargava Ram, S.I. Shkuratov, D. Aurongzeb, M. Holtz, J. Berg, J. Yun, H. Temkin, Appl. Phys. Lett. 84 (23) (2004) 4735–4737.
[16] I. Heilbron, H.J. Emeléus, H.W. Melville, A.R. Todd, M.A. Whiteley, A.J.E. Welch, L.N. Owen (Eds.), Thorpe's Dictionary of Applied Chemistry, vol. 11, 4th ed., Longmans, Green and Co. Ltd., London, 1965, p. 563.
[17] A.G. Merzhanov, Proceedings of the 14th International Colloquium on Dynamics of Explosions and Reactive Systems, vol. I, University of Coimbra, Coimbra, August 1–6, 1993, pp. 1–29.
[18] R. Orrù, B. Simoncini, D. Carta, G. Cao, Int. J. Self-Propag. High-Temp. Synth. 6 (1) (1997) 15–27.
[19] G. Cao, G. Concas, A. Corrias, R. Orrù, G. Paschina, B. Simoncini, G. Spano, Z. Naturforsch. 52a (1997) 539–549.
[20] R. Orrù, B. Simoncini, P.F. Virdis, G. Cao, Chem. Eng. Commun. 163 (1998) 23–35.
[21] G. Concas, A. Corrias, E. Manca, G. Marongiu, G. Paschina, G. Spano, Z. Naturforsch. 53a (1998) 239–244.

[22] R. Orrù, B. Simoncini, P.F. Virdis, G. Cao, Metall. Sci. Technol. 15 (1) (1997) 31–38.
[23] R. Orrù, B. Simoncini, P.F. Virdis, G. Cao, Metall. Sci. Technol. 14 (2) (1996) 69–77.
[24] H.J. Goldschmidt, Interstitial Alloys, Butterworths, London, 1967.
[25] J. Mei, R.D. Halldearn, P. Xiao, Scripta Mater. 41 (5) (1999) 541–548.
[26] P. Matteazzi, G. Le Caër, J. Am. Ceram. Soc. 75 (10) (1992) 2749–2755.
[27] P. Matteazzi, M. Alcalà, Mater. Sci. Eng. A 230 (1997) 161–170.
[28] D. Basset, P. Matteazzi, F. Miani, G. Le Caër, Hyperfine Interact. 94 (1994) 2235–2238.
[29] C. Cuadrado-Laborde, L.C. Damonte, L. Mendoza-Zélis, L.M. Socolovsky, I.L. Torriani, Physica B 354 (1–4) (2004) 125–128.
[30] C. Cuadrado-Laborde, L.C. Damonte, L. Mendoza-Zélis, Hyperfine Interact. 134 (2001) 131–140.
[31] G.F. Goya, H.R. Rechenberg, J. Phys.: Condens. Matter 12 (2000) 10579–10590.
[32] V.A. Shabashov, V.V. Sagaradze, A.V. Litvinov, A.G. Mukoseev, N.F. Vildanova, Mater. Sci. Eng. A 392 (2005) 62–72.
[33] N.N. Greenwood, T.C. Gibb, Mössbauer Spectroscopy, Chapman and Hall Ltd., London, 1971.
[34] M.G. Ferreira da Silva, B.F.O. Costa, J. Non-Cryst. Solids 293–295 (2001) 534–538.
[35] I.C.D.D. PDF2 Database, International Centre for Diffraction Data, Swarthmore, USA, 2000.
[36] L. Durães, J. Campos, A. Portugal, Propell. Explos. Pyrot. 31 (1) (2006) 42–49.
[37] S. Sarkar, C. Bansal, J. Alloys Compd. 334 (2002) 135–142.
[38] Z.Q. Gao, B. Fultz, Philos. Mag. B 67 (6) (1993) 787–800.
[39] M.R. Lesoille, P.M. Gielen, Phys. Stat. Sol. 37 (1970) 127–139.
[40] L. Durães, P. Brito, J. Campos, A. Portugal, in: W. Marquardt, C. Pantelides (Eds.), Proceedings of the 16th European Symposium on Computer Aided Process Engineering and Proceedings of the Ninth International Symposium on Process Systems Engineering, 21A of Comp. Aided Chem. Eng., Elsevier, Amsterdam, 2006, pp. 365–370.
[41] N.B. Dahotre, S. Nayak, Surf. Coat. Technol. 194 (2005) 58–67.
[42] S. Nayak, L. Riester, H.M. Meyer, N.B. Dahotre, J. Mater. Res. 18 (4) (2003) 833–839.
[43] C. McCammom, Mineral Physics and Crystallography: A Handbook of Physical Constants, American Geophysical Union, Washington, DC, 1995, pp. 332–347.
[44] M.J. Rossiter, J. Phys. Chem. Solids 26 (1965) 775–779.
[45] E. Gaffet, F. Bernard, J.C. Niepce, F. Charlot, C. Gras, G. Le Caër, J.L. Guichard, P. Delcroix, A. Mocellin, O. Tillement, J. Mater. Chem. 9 (1999) 305–314.